

iResum: a new paradigm for resumming gravitational wave amplitudes

Alessandro Nagar^{1,2} and Abhay Shah³

¹*Institut des Hautes Etudes Scientifiques, 91440 Bures-sur-Yvette, France*

²*INFN, Sez. di Torino, Via P. Giuria 1, 10125, Torino, Italy*

³*Mathematical Sciences, University of Southampton, Southampton, SO17 1BJ, United Kingdom*

(Dated: November 11, 2018)

We introduce a new, resummed, analytical form of the post-Newtonian (PN), factorized, multipolar amplitude corrections $f_{\ell m}$ of the effective-one-body (EOB) gravitational waveform of spinning, nonprecessing, circularized, coalescing black hole binaries (BBHs). This stems from the following two-step paradigm: (i) the *factorization* of the orbital (spin-independent) terms in $f_{\ell m}$; (ii) the *resumming* of the residual spin (or orbital) factors. We find that resumming the residual spin factor by taking its *inverse resummed* (iResum) is an efficient way to obtain amplitudes that are more accurate in the strong-field, fast-velocity regime. The performance of the method is illustrated on the $\ell = 2$ and $m = (1, 2)$ waveform multipoles, both for a test-mass orbiting around a Kerr black hole and for comparable-mass BBHs. In the first case, the iResum $f_{\ell m}$'s are much closer to the corresponding “exact” functions (obtained solving numerically the Teukolsky equation) up to the light-ring, than the nonresummed ones, especially when the black-hole spin is nearly extremal. The iResum paradigm is also more efficient than including higher post-Newtonian terms (up to 20PN order): the resummed 5PN information yields per se a rather good numerical/analytical agreement at the last-stable-orbit, and a well-controlled behavior up to the light-ring. For comparable mass binaries (including the highest PN-order information available, 3.5 PN), comparing EOB with Numerical Relativity (NR) data shows that the analytical/numerical fractional disagreement at merger, *without NR-calibration of the EOB waveform*, is generically reduced by iResum, from a 40% of the usual approach to just a few percents. This suggests that EOBNR waveform models for coalescing BBHs may be improved using iResum amplitudes.

PACS numbers: 04.30.Db, 04.25.Nx, 95.30.Sf, 97.60.Lf

I. INTRODUCTION

Determining the physical properties of the binary black hole (BBH) mergers GW150914 [1] and GW151226 [2] required a large bank of (semi)-analytical gravitational wave (GW) templates [3–5]. The effective-one-body (EOB) theory [3, 6–8] was essential to model gravitational waveforms from BBHs with total mass $M \equiv m_1 + m_2$ larger than $4M_\odot$ [9]. One of the pillars of EOB theory is the factorized and resummed (circularized) multipolar post-Newtonian (PN) waveform of Refs. [10, 11] (generalized to spinning binaries in [12]), that radically improves the 1997 pioneering work of Ref. [13] on PN fluxes resummation. The resummation makes this waveform better behaved in the strong-field, fast-velocity regime (i.e., up to merger), than the standard, Taylor-expanded, PN result [14] (the leading PN order being Einstein’s quadrupole formula). The squared waveform multipoles, summed together, give the GW angular momentum flux emitted at infinity (or absorbed at the horizons [6, 15, 16]) that provides the radiation reaction force driving the binary dynamics from the quasi-adiabatic circular inspiral through plunge and merger. This paper proposes an additional factorization (and resummation) of the (residual) multipolar waveform amplitude correction for nonprecessing, spinning, BBHs of Refs. [12, 17] to improve its behavior close to merger, both for large-mass-ratio and comparable-mass-ratio binaries, thus helping the development of EOB-based waveform models [3, 8]. We mostly use units with $c = G = 1$.

II. RESULTS: THE LARGE-MASS-RATIO LIMIT.

The factorized multipolar waveform for circularized, nonprecessing, BBHs with total mass M and spins S_1 and S_2 reads (see e.g. Eq.(75)-(78) of [6])

$$h_{\ell m}(x) = h_{\ell m}^{(N, \epsilon)} \hat{h}_{\ell m}^{\text{tail}} \hat{S}_{\text{eff}}^{(\epsilon)} f_{\ell m}(x, S_1, S_2), \quad (1)$$

where $x = (GM\Omega/c^3)^{2/3} = \mathcal{O}(c^{-2})$ is the PN-ordering frequency parameter [we recall that n -PN order means $\mathcal{O}(c^{-2n})$ in the equations of motion], $h_{\ell m}^{(N, \epsilon)}$ the Newtonian prefactor, where $\epsilon = 0, 1$ is the parity of the considered multipole, i.e. of $\ell + m$ (see also Eq. (78) of [6]); $\hat{h}_{\ell m}^{\text{tail}} \equiv T_{\ell m} e^{i\delta_{\ell m}}$ is the (complex) factor that accounts for the effect of tails [10, 11]; the third factor, $\hat{S}_{\text{eff}}^{(\epsilon)}$ is the usual parity-dependent source term defined as the effective EOB Hamiltonian when $\epsilon = 0$ or the Newton-normalized orbital angular momentum when $\epsilon = 1$ [11]. The fourth factor, $f_{\ell m}$, is the residual amplitude correction; its further resummation when $\nu \equiv m_1 m_2 / M^2 \neq 0$ and $S_{1,2} \neq 0$, depends on the parity of m [3, 8]. When m is even, it is resummed as $f_{\ell m} = (\rho_{\ell m})^\ell$ with $\rho_{\ell m}$ given as

$$\rho_{\ell m} = \rho_{\ell m}^{\text{orb}} + \rho_{\ell m}^{\text{S}}, \quad (2)$$

where $\rho_{\ell m}^{\text{orb}}$ is the *orbital* (spin-independent) contribution and $\rho_{\ell m}^{\text{S}}$ is the spin-dependent part. Both functions are given as PN-expansions. The PN-accuracy of $\rho_{\ell m}$'s

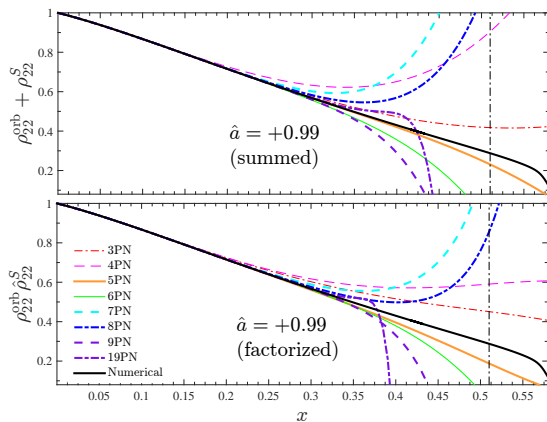


FIG. 1. Large-mass-ratio limit, BH spin $\hat{a} = +0.99$: various PN approximants of ρ_{22} with additive spin-dependence (top, Eq. (2)) or factorized (bottom, Eq. (3)). Increasing the PN order does not reduce the (large) disagreement with the numerical (“exact”) curve towards the LSO (vertical line). The x -axis ends at the light-ring frequency.

currently used in EOB models [3, 8] is relatively low: $\rho_{\ell m}^{\text{orb}}$ is taken at 3^{+2} PN accuracy [18] (i.e., up to 3PN with complete mass-ratio dependence plus 4PN and 5PN test-particle, $\nu = 0$, terms) while $\rho_{\ell m}^{\text{S}}$, e.g., as used in the SEOB_ihes model [6, 8], has leading-order (LO, i.e. 2PN) spin-spin (S^2) terms and up to next-to-leading-order (NLO, i.e. 2.5PN) spin-orbit (SO) terms. Thanks to recent analytical work [19–21], the $f_{\ell m}$ ’s (for both even and odd m ’s) can be obtained up to next-to-next-to-leading-order (NNLO) in SO, NLO in S^2 and LO in S^3 . In the large-mass-ratio (i.e., test-particle) case ($m_1 \gg m_2$, i.e. $\nu = 0$), $\rho_{\ell m}^{\text{orb}}$ is known at 22.5PN [22]; for a spinning BH, the fluxes were obtained at 20PN [23] extracting the PN coefficients from numerical data (see also Ref. [22] for a fully analytical calculation at 11PN).

Let us first focus on the (nonspinning) test-particle case, $m_2 \ll m_1$, around a spinning BH. We shall use dimensionless spin variables $\hat{a}_{1,2} \equiv S_{1,2}/(m_{1,2})^2$, which in the non-spinning test-particle case yield $\hat{a}_2 = 0$ and $\hat{a} \equiv \hat{a}_1$. We discuss here explicitly only the $\ell = m = 2$ and $\ell = 2, m = 1$ modes, postponing elsewhere the investigation of other multipoles. From the 20PN flux of Ref. [23], we obtain the 20PN-accurate ρ_{22} , as in Eq. (2), and explore its behavior for the most demanding case $\hat{a} = +0.99$ (our conclusions actually hold for any smaller value of \hat{a}). Figure 1, top, contrasts various PN-approximants ρ_{22} with the “exact” (numerical) curve ρ_{22}^{Num} (black) stopping at the light-ring. This curve was factorized from the energy fluxes computed by S. Hughes solving numerically the Teukolsky equation with high accuracy (fractional uncertainty 10^{-14}) [16]. The vertical dash-dotted line marks the last-stable-orbit (LSO). The overall bad behavior of the various PN-approximants is evident, with the 19PN one (as an example of high-PN information) not showing any improvement with respect to any lower-PN curve. The strong-field inaccuracy of the

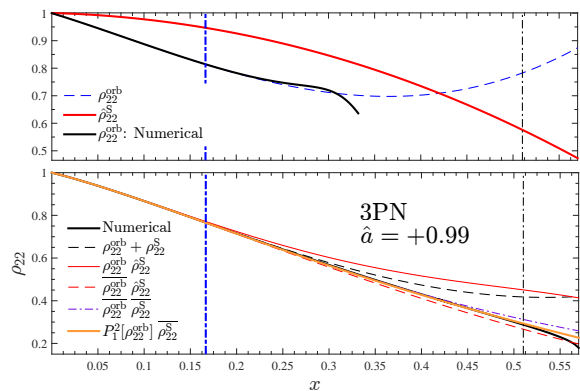


FIG. 2. Large-mass-ratio limit, 3PN accuracy. Top: the behavior of the two factors ρ_{22}^{orb} and $\hat{\rho}_{22}^{\text{S}}$. The zero-spin (orbital), exact, curve (black, ending at the Schwarzschild light-ring, $x = 1/3$) is included for comparison. Bottom: comparing nonresummed and resummed functions. Note the improvement towards LSO (and beyond) due to resummations.

PN-expanded ρ_{22} when $\hat{a} \gtrsim 0.7$ was already noted (at 4PN only) in [12] and improvements were proposed (see also [22, 24, 25]), though fine-tuned to the test-particle limit.

To devise a new form of ρ_{22} that is well-behaved up to the light-ring and valid also beyond the test-particle case, we: (i) *factorize* the orbital part and (ii) *resum* the resulting spin (or orbital) factors. At n -PN order the *orbital factorized* amplitudes read

$$\tilde{\rho}_{\ell m}(x; \hat{a}) \equiv \rho_{\ell m}^{\text{orb}} \hat{\rho}_{\ell m}^{\text{S}}, \quad (3)$$

where $\hat{\rho}_{\ell m}^{\text{S}} \equiv T_n [1 + \rho_{\ell m}^{\text{S}}(x; \hat{a})/\rho_{\ell m}^{\text{orb}}(x)]$, with $T_n[\dots]$ denoting the Taylor expansion at order n . The 5PN $\hat{\rho}_{22}^{\text{S}}$ reads

$$\begin{aligned} \hat{\rho}_{22}^{\text{S}_{5\text{PN}}} = & 1 - \frac{2}{3}\hat{a}x^{3/2} + \frac{\hat{a}^2}{2}x^2 - \frac{145}{63}\hat{a}x^{5/2} + \frac{109}{126}\hat{a}^2x^3 \\ & + \left(-\frac{9808}{3969}\hat{a} + \frac{\hat{a}^3}{3}\right)x^{7/2} + \left(\frac{7207}{2646}\hat{a}^2 - \frac{\hat{a}^4}{8}\right)x^4 \\ & + \left[\frac{925}{1134}\hat{a}^3 + \hat{a}\left(-\frac{5094410}{305613} + \frac{16}{3}\text{eulerlog}_2(x)\right)\right]x^{9/2} \\ & + \left(\frac{1753858}{305613}\hat{a}^2 - \frac{59}{252}\hat{a}^4\right)x^5, \end{aligned} \quad (4)$$

where $\text{eulerlog}_2(x) = \gamma + 2 \log 2 + 1/2 \log x$; the 5PN ρ_{22}^{orb} is given in Eq. (50) of [11]. To understand how to proceed further, let us take the 3PN-truncations of $(\rho_{22}^{\text{orb}}, \rho_{22}^{\text{S}})$ for $\hat{a} = +0.99$, see Fig. 2, top. The bottom panel contrasts the exact curve with various ways of using this 3PN information.

Inspecting Fig. 2, one sees that up to, say, the Schwarzschild LSO frequency, $x_{\text{LSO}}^{\text{Schw}} = 1/6 = 0.1\bar{6}$ (thick, blue, vertical line), ρ_{22}^{orb} and ρ_{22}^{S} somehow compensate each other, so that their product $\rho_{22}^{\text{orb}} \hat{\rho}_{22}^{\text{S}}$ is on top of ρ_{22}^{Num} . For larger values of x , the orbital factor takes over to determine a large difference at $x_{\text{LSO}}^{+0.99}$ (thinner vertical

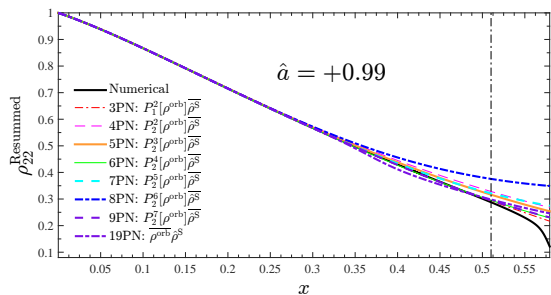


FIG. 3. Resumming separately ρ_{22}^{orb} and $\hat{\rho}_{22}^{\text{S}}$: the reduction of the PN ambiguity towards the LSO (vertical line) as well as the closeness to the numerical curve is remarkable (and consistent) for any PN order (contrast with Fig. 1).

line in Fig. 2). The behavior of the 3PN-accurate ρ_{22}^{orb} and $\hat{\rho}_{22}^{\text{S}}$ remains essentially unchanged also at higher PN orders (see Fig. 1, bottom), with the orbital factor dominating when the $\hat{\rho}_{22}^{\text{S}}$'s increase towards the LSO, and the spin factor dominating when they decrease and get negative [?]. Both (ρ_{22}^{orb} and $\hat{\rho}_{22}^{\text{S}}$) can be separately improved by replacing them with suitable resummed expressions, so that their growth (or decrease) is milder towards $x_{\text{LSO}}^{+0.99}$; this eventually reduces the global disagreement of their product with ρ_{22}^{Num} . There are several ways of doing so. A simple approach is to resum one of the two factors (or both) by taking its inverse, i.e. replacing a function $f(x)$ with its inverse resummed (the “iResum”) representation

$$\overline{f(x)} \equiv (T_n [(f(x))^{-1}])^{-1}. \quad (5)$$

Figure 2, bottom, illustrates the remarkable efficiency of this procedure when it is applied just to ρ_{22}^{orb} (red-dashed line) or to both ρ_{22}^{orb} and $\hat{\rho}_{22}^{\text{S}}$ (purple, dash-dotted line). An even better approximant even beyond the LSO is obtained by taking the (2,1) Padé approximant of ρ_{22}^{orb} multiplied by $\hat{\rho}_{22}^{\text{S}}$. It is remarkable that the 3PN information, once properly resummed, can yield accurate predictions (1% fractional difference) for such an extremal value of \hat{a} [?]. The method consistently works up to 9PN, so that the large PN-ambiguity of Fig. 1 is dramatically reduced, see Fig. 3. For n -PN order, we always take the $(n-2, 2)$ Padé approximant of ρ_{22}^{orb} , since it is the only one without spurious poles. We also note that, up to 5PN, also functions of the form $\overline{\rho_{22}^{\text{orb}}} \hat{\rho}_{22}^{\text{S}}$ are rather accurate up to $x_{\text{LSO}}^{+0.99}$. Unfortunately, the same is not true up to 9PN because of a pole in $\overline{\rho_{22}^{\text{orb}}}$ that progressively moves within the x -domain of interest; it is however possible to take $\overline{\rho_{22}^{\text{orb}}} \hat{\rho}_{22}^{\text{S}}$ instead, although globally its performance is slightly worse than that of Fig. 3 (as for 7PN and 8PN). For higher PN ($10 \leq n \leq 20$) the simple recipes discussed above yield, on average, less good and less robust results. The only exception is given by the 19PN, that can be consistently resummed as $\overline{\rho_{22}^{\text{orb}}} \hat{\rho}_{22}^{\text{S}}$ (see Fig. 3). Summarizing, any PN-resummed function of Fig. 3 can be used to construct reliable radiation reaction for BBH

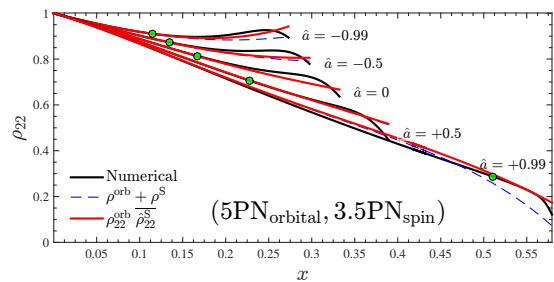


FIG. 4. Large mass-ratio limit: ρ_{22}^{orb} at 5PN and ρ_{22}^{S} at 3.5PN. Resumming only the spin-dependent factor yields a remarkable agreement with the numerical curve through LSO (and beyond), notably when $\hat{a} \approx 1$.

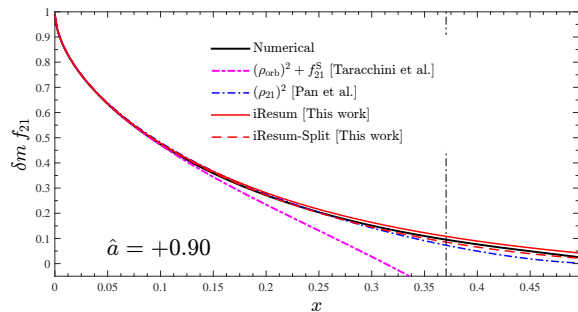


FIG. 5. Large mass-ratio limit, $\hat{a} = +0.9$. Contrasting various representation of $\delta m f_{21}$, with 5PN-accurate ρ_{21}^{orb} and 2.5PN-accurate f_{21}^{S} . The x -axis ends at the light-ring and the vertical line marks the LSO. The defactorized amplitude of [6, 17], Eq. (6), is largely inaccurate; by contrast, any of its resummed versions (obtained taking the inverse of spin-dependent parts) remains rather close to the exact one up to the light-ring.

coalescence in the test-particle limit [26, 27] so to improve several results (see e.g. [27, 28]) that are biased by its poor accuracy for high spins [?].

To prepare the ground for the $\nu \neq 0$ case, where ρ_{22}^{orb} is taken at 3⁺ PN and ρ_{22}^{S} at 3.5PN (i.e., including NNLO SO, NLO in S^2 and LO S^3 , see Eq. (4)) we want to explore the efficiency of iResum also with this particular PN truncation. Although the above analyses suggest to resum both $\rho_{\ell m}^{\text{orb}}$ and $\hat{\rho}_{\ell m}^{\text{S}}$ also when $\nu \neq 0$ for consistency, here we do it only on $\hat{\rho}_{\ell m}^{\text{S}}$, keeping $\rho_{\ell m}^{\text{orb}}$ non-resummed, as it is in well-established, NR-calibrated, EOBNR nonspinning models [8]. We take then $\overline{\rho_{22}^{\text{orb}}}$ at 5PN and $\hat{\rho}_{22}^{\text{S}}$ at 3.5PN and replace $\hat{\rho}_{22}^{\text{S}}$ with $\overline{\hat{\rho}_{22}^{\text{S}}}$. Figure 4 illustrates the quality of this choice for a few values of $\hat{a} \in [-0.99, 0.99]$. The plot also exhibits the additive $\overline{\rho_{22}^{\text{orb}}} \overline{\hat{\rho}_{22}^{\text{S}}}$ of Eq. (2). The filled circles indicate LSO frequencies. The numerical-analytical fractional difference is at most of 6% before the LSO for $\hat{a} = +0.99$, and always smaller for other values of \hat{a} (we also checked the agreement for other intermediate values of \hat{a} , not shown in the plot). The fractional difference at LSO is 3% for $\hat{a} = +0.99$, 1% for $\hat{a} = 0.7$ and $\leq 0.2\%$ when $\hat{a} \leq 0.5$.

Implementing a similar procedure when m is odd calls for some distinctions. Following Refs. [6, 17], the straight-

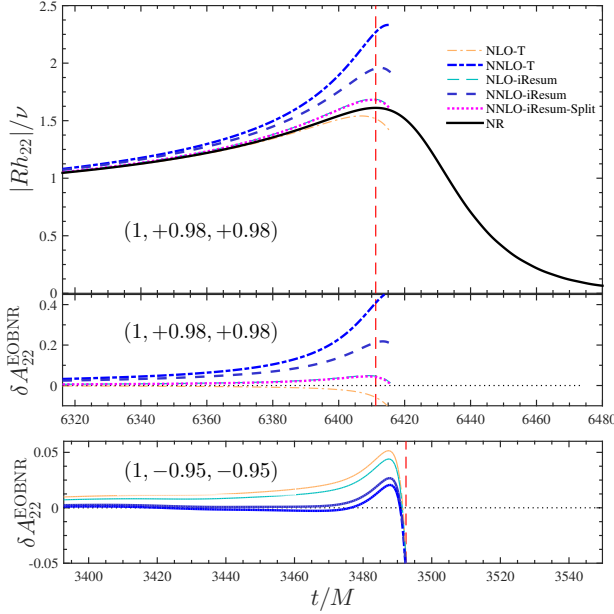


FIG. 6. Equal-mass, equal-spin case, EOB/NR comparison: the spread between NNLO and NLO is smaller for iResum than for the Taylor-expanded (T) residual amplitudes. The iResum waveform is always closer to the NR one at merger (red vertical line).

forward computation of $\rho_{\ell m}$ as when m is even, though doable in the test-particle limit, is unfit to the equal-mass case, because of formally singular terms. The solution [6, 17], is to *defactorize* the equal-mass vanishing factor, $X_{12} \equiv X_1 - X_2 = \delta m = (m_1 - m_2)/M$, from $h_{\ell m}^N$ and use instead

$$\delta m f_{\ell m}(x, S_1, S_2) = X_{12} (\rho_{\ell m}^{\text{orb}})^\ell + \tilde{f}_{\ell m}^S \quad (6)$$

where the X_{12} -rescaled functions $\tilde{f}_{\ell m}^S$, are given, at NLO, in Eqs. (90)-(94) of [6]. In the test-particle limit ($\nu = 0$ and $X_{12} = 1$), the \hat{a} -dependence up to 3.5PN is given in Eq. (28b) of [12]. Following the same rationale behind choosing 5PN+3.5PN for the (2, 2) mode, we take ρ_{21}^{orb} at 5PN and \tilde{f}_{21}^S at 2.5PN, because this is the highest-PN spin term known with $\nu \neq 0$ (see below). Figure 5 refers to $\hat{a} = +0.9$, and illustrates the large disagreement between $\delta m f_{21}$ of Eq. (6) and $\delta m f_{21}^{\text{Num}}$ built up to the LSO (vertical line). One can improve $\delta m f_{21}$ as in the m -even case: (i) by factoring $(\rho_{\ell m}^{\text{orb}})^\ell$ and defining

$$\delta m \tilde{f}_{\ell m} = (\rho_{\ell m}^{\text{orb}})^\ell \tilde{f}_{\ell m}^S, \quad (7)$$

where $\tilde{f}_{\ell m}^S \equiv T_N [X_{12} + \tilde{f}_{\ell m}^S / (\rho_{\ell m}^{\text{orb}})^\ell]$, and (ii) by resumming this latter taking its inverse, Eq. (5). The result (red, solid, line in Fig. 5) remains very close to the numerical curve up to light-ring. Figure 5 also illustrates (blue line, dash-dotted) the performance of the “standard” $f_{21} = (\rho_{21})^2$ as given by Eq. (29b) of Pan et al. [12], without any additional resummation [?].

III. RESULTS: THE $\nu \neq 0$ CASE.

We obtained the ν -dependent $\hat{\rho}_{22}^S$ and \hat{f}_{21}^S at the highest present PN accuracy from the multipolar decomposition of the total flux (given to us by S. Marsat and A. Bohe from their summed result [19, 21]) that is known at NNLO, NLO and LO for SO, S^2 and S^3 terms respectively. Expressions are simplified using $\tilde{a}_{1,2} \equiv X_{1,2} \hat{a}_{1,2} = S_{1,2}/(Mm_{1,2})$, $\hat{a}_0 \equiv \tilde{a}_1 + \tilde{a}_2$ and $\tilde{a}_{12} \equiv \tilde{a}_1 - \tilde{a}_2$, so to get

$$\begin{aligned} \hat{\rho}_{22}^S = & 1 - \left[\frac{\hat{a}_0}{2} + \frac{1}{6} X_{12} \tilde{a}_{12} \right] x^{3/2} + \frac{1}{2} \hat{a}_0^2 x^2 \\ & + \left[\left(-\frac{337}{252} + \frac{73}{252} \nu \right) \hat{a}_0 - X_{12} \tilde{a}_{12} \left(\frac{27}{28} + \frac{11}{36} \nu \right) \right] x^{5/2} \\ & + \left[\frac{221}{252} X_{12} \tilde{a}_{12} \hat{a}_0 - \hat{a}_0^2 \left(\frac{1}{84} + \frac{31}{252} \nu \right) \right] \\ & \times \left(1 - \frac{\tilde{a}_1 \tilde{a}_2}{\hat{a}_0^2} \frac{264 - 103\nu}{3 + 31\nu} \right) x^3 + \left[\hat{a}_0 \left(-\frac{2083}{2646} \right. \right. \\ & + \left. \frac{123541}{10584} \nu + \frac{4717}{2646} \nu^2 \right) + X_{12} \tilde{a}_{12} \left(-\frac{13367}{7938} \right. \\ & + \left. \frac{22403}{15876} \nu + \frac{25}{324} \nu^2 \right) + \frac{7}{12} \hat{a}_0^3 - \frac{1}{4} X_{12} \tilde{a}_{12} \hat{a}_0^2 \left. \right] x^{7/2}, \quad (8) \end{aligned}$$

and

$$\hat{f}_{21}^S = X_{12} f_0^S - \frac{3}{2} \tilde{a}_{12} x^{1/2} f_1^S, \quad (9)$$

where

$$\begin{aligned} f_0^S = & 1 - \frac{13}{84} \hat{a}_0 x^{3/2} + \frac{3}{8} \hat{a}_0^2 \left(1 + \frac{4}{3} \frac{\tilde{a}_1 \tilde{a}_2}{\hat{a}_0^2} \right) x^2 \\ & + \hat{a}_0 \left(-\frac{14705}{7056} + \frac{12743}{7056} \nu \right) x^{5/2}, \quad (10) \end{aligned}$$

$$\begin{aligned} f_1^S = & 1 - \left(\frac{349}{252} + \frac{74}{63} \nu \right) x \\ & + \frac{9}{4} \hat{a}_0 x^{3/2} - \left(\frac{3379}{21168} - \frac{4609}{10584} \nu + \frac{39}{392} \nu^2 \right) x^2, \quad (11) \end{aligned}$$

and the S^3 term is here omitted for simplicity. Figures 6 and 7 illustrate the benefits of iResum when applied to (truncations of) the above expressions. The figures compare EOB waveform amplitudes to NR waveform amplitudes from the SXS catalog [29] for a few meaningful choices of mass ratio and spins. For all EOB waveforms, the underlying EOB dynamics is that of the `SEOBNR_ihcs` model of Ref. [8], with the NR-calibration of the parameters $(a_6^c(\nu), c_3(\tilde{a}_1, \tilde{a}_2, \nu))$ provided by Eqs. (5) and (11) therein. By contrast, the waveform is *purely analytical* without the NR-calibrated next-to-quasi-circular (NQC) factors and ringdown (see [8] for the performance of the full EOB waveform), that is why it stops just after merger (dashed vertical line). The figures also include EOB-NR fractional differences, i.e. $\delta A_{\ell m}^{\text{EOBNR}} \equiv (A_{\ell m}^{\text{EOB}} -$

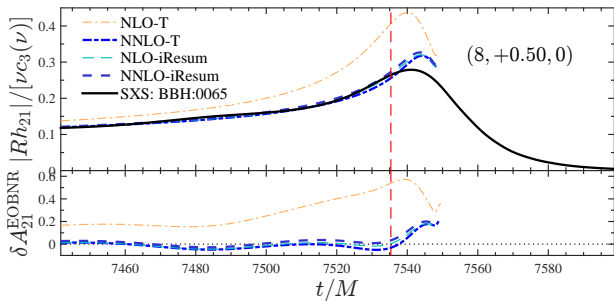


FIG. 7. Same NNLO/NLO/NR comparison as Fig. 6, but for the (2,1) mode, mass ratio $m_1/m_2 = 8$ and spins $(\hat{a}_1, \hat{a}_2) = (+0.5, 0)$. The efficiency of iResum on NLO is remarkable.

$A_{\ell m}^{\text{NR}}/A_{\ell m}^{\text{NR}}$, where $A_{\ell m} \equiv |Rh_{\ell m}|$. For $(\ell, m) = (2, 2)$ the waves are aligned using a standard procedure [8] during the early inspiral; for (2,1) around merger, so to better highlight the differences there. With the label NLO we actually indicate the spin information included in [8], i.e. NLO in the SO sector and LO *only* in SS, while NNLO refers to the complete Eqs. (8)-(11) above. We obtained $\hat{\rho}_{22}^{\text{S}}$ likewise the $\nu = 0$ case. To iResum \hat{f}_{21}^{S} , instead, we replace the Taylor-expansions $(f_0^{\text{S}}, f_1^{\text{S}})$ in Eq. (9) by $(\hat{f}_0^{\text{S}}, \hat{f}_1^{\text{S}})$, because $X_{12} = 0$ when $\nu = 1/4$ and thus the direct inverse resummation of \hat{f}_{21}^{S} is singular at $\nu = 1/4$. To validate this procedure we applied it to the test-particle limit of Eq. (9) (i.e., without the \hat{a}^3 term) finding again a remarkable agreement with f_{21}^{Num} (see red-dashed line in Fig. 5) all over.

Figures 6-7 show that: (i) for (2,2) mode the effect of iResum (both at NLO and NNLO level) is to reduce NR/EOB gap at merger as well as the difference between NLO and NNLO approximants; surprisingly, even with iResum, the NR/EOB difference *is not* smaller at NNLO than at NLO (especially for $\hat{a}_1 = \hat{a}_2 = +0.98$). This is due to the excessive growth of $\hat{\rho}_{22}^{\text{S}}$ that is not compensated by the (decreasing) ρ_{22}^{orb} . Interestingly, the problem can be solved proceeding similarly to \hat{f}_{21}^{S} , i.e., writing Eq. (8) as $\hat{\rho}_{22}^{\text{S}} = (1 - \frac{\hat{a}_0}{2}x^{3/2} + \dots) - \frac{1}{6}X_{12}\tilde{a}_{12}x^{3/2}(1 - \frac{221}{42}\hat{a}_0x^{3/2} + \dots)$ and then iResumming separately each $1 + \dots$ piece. The result (magenta lines in Fig. 6), shows

perfect consistency between NLO and NNLO and suggests that the NNLO information has actually little impact; (ii) Fig. 7 tells a similar story for the (2,1) mode (for a different binary though, since $h_{21} = 0$ for $m_1 = m_2$ and $\hat{a}_1 = \hat{a}_2$), with the iResum NLO well consistent within the NR waveform error (typically, of a few percents) and essentially comparable to (any of) the NNLO amplitudes.

IV. CONCLUSIONS

Our results (both for $\nu \neq 0$ and $\nu = 0$) indicate that iResum waveforms may be better analytical choice for EOB/NR models, with little NR-tuned additional modifications (e.g., by fixing the NQC factors [8]) needed to obtain an excellent EOB/NR amplitude agreement at merger. Our approach looks particularly promising (and in fact needed) to easily improve subdominant multipoles (as the (2,1), discussed in detail) that are currently (mostly) missing in EOB/NR waveform models. The resummation of the other subdominant multipoles, as well as their consistent implementation in `SEOBNR_ihes`, so as to improve both the waveform and the radiation reaction, will be discussed in future work

ACKNOWLEDGMENTS

We are very grateful to S. Hughes for providing us with the numerical fluxes used to compute $(\rho_{\ell m}^{\text{Num}}, f_{21}^{\text{Num}})$. We warmly thank A. Bohé, G. Faye and S. Marsat for computing for us the multipolar decomposition of their PN total fluxes. A. N. is very much indebted to: D. Hilditch for discussions that occurred long ago and that eventually helped to shape a concept; to E. Harms to compute and test, at a very early stage of this work, the behavior of the standard ρ_{22} up to 14PN; and T. Damour for discussions and timely constructive criticisms. A. S. thanks IHES for hospitality at various stages of development of this work. This work was supported in part by the European Research Council under the European Union's Seventh Framework Programme (FP7/2007-2013)/ERC grant agreement no. 304978.

-
- [1] B. P. Abbott et al. (Virgo, LIGO Scientific), Phys. Rev. Lett. **116**, 061102 (2016), 1602.03837.
 - [2] B. P. Abbott et al. (Virgo, LIGO Scientific), Phys. Rev. Lett. **116**, 241103 (2016), 1606.04855.
 - [3] A. Taracchini, A. Buonanno, Y. Pan, T. Hinderer, M. Boyle, et al., Phys.Rev. **D89**, 061502 (2014), 1311.2544.
 - [4] S. Husa, S. Khan, M. Hannam, M. Puerrer, F. Ohme, X. Jimnez Forteza, and A. Bohé, Phys. Rev. **D93**, 044006 (2016), 1508.07250.
 - [5] S. Khan, S. Husa, M. Hannam, F. Ohme, M. Puerrer, X. Jimnez Forteza, and A. Bohé, Phys. Rev. **D93**, 044007 (2016), 1508.07253.
 - [6] T. Damour and A. Nagar, Phys.Rev. **D90**, 044018 (2014), 1406.6913.
 - [7] B. Szilgyi, J. Blackman, A. Buonanno, A. Taracchini, H. P. Pfeiffer, M. A. Scheel, T. Chu, L. E. Kidder, and Y. Pan, Phys. Rev. Lett. **115**, 031102 (2015), 1502.04953.
 - [8] A. Nagar, T. Damour, C. Reisswig, and D. Pollney, Phys. Rev. **D93**, 044046 (2016), 1506.08457.

- [9] B. P. Abbott et al. (Virgo, LIGO Scientific), *Phys. Rev. Lett.* **116**, 241102 (2016), 1602.03840.
- [10] T. Damour and A. Nagar, *Phys. Rev.* **D76**, 064028 (2007), 0705.2519.
- [11] T. Damour, B. R. Iyer, and A. Nagar, *Phys. Rev.* **D79**, 064004 (2009).
- [12] Y. Pan, A. Buonanno, R. Fujita, E. Racine, and H. Tagoshi, *Phys.Rev.* **D83**, 064003 (2011), 1006.0431.
- [13] T. Damour, B. R. Iyer, and B. S. Sathyaprakash, *Phys. Rev.* **D57**, 885 (1998), gr-qc/9708034.
- [14] L. Blanchet, *Living Rev.Rel.* **17**, 2 (2014), 1310.1528.
- [15] A. Nagar and S. Akcay, *Phys.Rev.* **D85**, 044025 (2012), 1112.2840.
- [16] A. Taracchini, A. Buonanno, S. A. Hughes, and G. Khanna, *Phys.Rev.* **D88**, 044001 (2013), 1305.2184.
- [17] A. Taracchini, Y. Pan, A. Buonanno, E. Barausse, M. Boyle, et al., *Phys.Rev.* **D86**, 024011 (2012), 1202.0790.
- [18] T. Damour and A. Nagar, *Phys. Rev.* **D79**, 081503 (2009).
- [19] S. Marsat, L. Blanchet, A. Bohé, and G. Faye (2013), 1312.5375.
- [20] S. Marsat, *Class. Quant. Grav.* **32**, 085008 (2015), 1411.4118.
- [21] A. Bohé, G. Faye, S. Marsat, and E. K. Porter, *Class. Quant. Grav.* **32**, 195010 (2015), 1501.01529.
- [22] R. Fujita, *PTEP* **2015**, 033E01 (2015), 1412.5689.
- [23] A. G. Shah, *Phys. Rev.* **D90**, 044025 (2014), 1403.2697.
- [24] S. Isoyama, R. Fujita, N. Sago, H. Tagoshi, and T. Tanaka, *Phys. Rev.* **D87**, 024010 (2013), 1210.2569.
- [25] N. K. Johnson-McDaniel, *Phys. Rev.* **D90**, 024043 (2014), 1405.1572.
- [26] A. Taracchini, A. Buonanno, G. Khanna, and S. A. Hughes (2014), 1404.1819.
- [27] E. Harms, S. Bernuzzi, A. Nagar, and A. Zenginoglu (2014), 1406.5983.
- [28] A. Nagar, E. Harms, S. Bernuzzi, and A. Zenginolu, *Phys. Rev.* **D90**, 124086 (2014), 1407.5033.
- [29] <http://www.black-holes.org/waveforms>.
- [30] E. Harms, G. Lukes-Gerakopoulos, S. Bernuzzi, and A. Nagar, *Phys. Rev.* **D93**, 044015 (2016), 1510.05548.
- [31] S. E. Gralla, S. A. Hughes, and N. Warburton, *Class. Quant. Grav.* **33**, 155002 (2016), 1603.01221.